



# HOKKAIDO UNIVERSITY

Title	Direct Detection of the Substrate Uptake and Release Reactions of the Light-Driven Sodium-Pump Rhodopsin
Author(s)	Murabe, Keisuke; Tsukamoto, Takashi; Aizawa, Tomoyasu et al.
Citation	Journal of the American Chemical Society, 142(37), 16023-16030 <a href="https://doi.org/10.1021/jacs.0c07264">https://doi.org/10.1021/jacs.0c07264</a>
Issue Date	2020-09-16
Doc URL	<a href="https://hdl.handle.net/2115/82685">https://hdl.handle.net/2115/82685</a>
Rights	This document is the Accepted Manuscript version of a Published Work that appeared in final form in Journal of the American Chemical Society, copyright © American Chemical Society after peer review and technical editing by the publisher. To access the final edited and published work see <a href="https://doi.org/10.1021/jacs.0c07264">https://doi.org/10.1021/jacs.0c07264</a> .
Type	journal article
File Information	Revised manuscript.pdf



# Direct detection of the substrate uptake and release reactions of the light-driven sodium-pump rhodopsin

Keisuke Murabe,<sup>†</sup> Takashi Tsukamoto,<sup>†,§</sup> Tomoyasu Aizawa,<sup>†,§</sup> Makoto Demura,<sup>†,§</sup> and

Takashi Kikukawa<sup>\*,†,§</sup>

<sup>†</sup>Faculty of Advanced Life Science, Hokkaido University, Sapporo, 060-0810, Japan

<sup>§</sup>Global Station for Soft Matter, Global Institution for Collaborative Research and Education, Hokkaido University, Sapporo, 001-0021, Japan

---

**ABSTRACT:** For membrane transporters, substrate uptake and release reactions are major events during their transport cycles. Despite the functional importance of these events, it is difficult to identify their relevant structural intermediates because of the requirements of the experimental methods, which are to detect the timing of the formation and decay of intermediates and to detect the timing of substrate uptake and release. We report successfully achieving this for the light-driven Na<sup>+</sup> pump rhodopsin (NaR). Here, a Na<sup>+</sup>-selective membrane, which consists of polyvinyl chloride and a Na<sup>+</sup> ionophore, was employed to detect Na<sup>+</sup> uptake and release. When one side of the membrane was covered by the lipid-reconstituted NaR, continuous illumination induced an increase in membrane potential, reflecting Na<sup>+</sup> uptake by the photolyzed NaR. By using nanosecond laser pulses, two kinds of data were obtained during a single transport cycle: one was the flash-induced absorbance change in NaR in order to detect the formation and decay of structural intermediates, and the other was the flash-induced change in membrane potential, which reflects the transient Na<sup>+</sup> uptake and release reactions. Their comparison clearly indicated that Na<sup>+</sup> is captured and released during the formation and decay of the O intermediate, the redshifted intermediate which appears in the latter half of the transport cycle.

---

## INTRODUCTION

Membrane transport proteins play crucial roles in living cells by moving various molecules across the cell membranes. These transports are accomplished through multiple steps associated with structural intermediates. Among these steps, the substrate uptake and release are the major events and involve strategic conformational changes as proposed by the alternating access model<sup>1</sup>. During these events, the transporter is considered to alternate between an extracellular- and an intracellular-facing intermediate in which the substrate-binding site is accessible to only one side of the membrane. Thus, these intermediates should be identified and then analyzed to obtain a deeper understanding of the transport mechanisms. However, these identifications are difficult in most cases due to the necessity of measuring two aspects: One is to detect the timing of the formation and decay of respective intermediates, and the other is to detect the timing of substrate uptake and release. Here, we report a direct identification of the intermediates for the Na<sup>+</sup>-pump rhodopsin (NaR).

Rhodopsins are photoactive membrane proteins widely spread in all three domains of life<sup>2-3</sup>. According to the conserved residues, they are classified into two groups. One is animal rhodopsin, most of which act as photosensors like visual pigments in the eyes. The other is microbial rhodopsin found in unicellular microorganisms that performs divergent functions, such as light-driven ion pumps, light-signal transductions, light-gated ion channels, and even light-switchable enzymes. Among these, ion-pump rhodopsins are the most abundant and widely distributed in the microbial world. NaR was the third discovered

ion-pump rhodopsin and is considered to function in a significantly different manner from the other two ion pumps, the H<sup>+</sup> pump and Cl<sup>-</sup> pump, as described below<sup>4</sup>.

All microbial rhodopsins are composed of seven transmembrane helices and a chromophore retinal bound to a specific Lys residue via Schiff base linkage. Upon illumination, retinal isomerizes from an all-*trans* to a 13-*cis* configuration, distorting the protein conformation. This energized intermediate state thermally relaxes to the original state through various structural intermediates. During these cyclic reactions called photocycles, microbial rhodopsins perform their respective functions.

In the dark states, the Schiff bases are commonly protonated. The resultant positive charges are a prerequisite for both visible light absorption and the light-induced functions themselves. These protonated Schiff bases (PSBs) are also utilized in ion pumps. For the H<sup>+</sup> pump, the first H<sup>+</sup> transfer occurs from PSB to a nearby Asp residue upon illumination<sup>5-6</sup>. This H<sup>+</sup> transfer is essential to drive the multiple subsequent H<sup>+</sup> transfer reactions, which finally accomplish active H<sup>+</sup> transport across the cell membrane. For the Cl<sup>-</sup> pump, the substrate Cl<sup>-</sup> binds in the vicinity of a Schiff base NH<sup>+</sup>, which is oriented toward the extracellular (EC) side<sup>7-8</sup>. Upon photoinduced isomerization, the NH<sup>+</sup> turns toward the cytoplasmic (CP) side, which results in driving the Cl<sup>-</sup> into the CP channel. The PSB is a prerequisite for Cl<sup>-</sup> binding and thus essential for Cl<sup>-</sup> pump function<sup>9</sup>. Different from Cl<sup>-</sup>, cations cannot bind near the PSB due to the repulsion between the positive charges. Thus, microbial rhodopsin has been considered to be unable to pump cations

(other than  $H^+$ ) before the discovery of NaR<sup>10-11</sup>. Indeed, for the nonphotolyzed NaR, the substrate  $Na^+$  has not been identified in the vicinity of the PSB<sup>11-13</sup>. Nevertheless, NaR can pump  $Na^+$  outward.

Previous studies on NaR showed that the substrate  $Na^+$  is transiently captured after illumination and then released before the end of the photocycle<sup>11</sup>. However, these uptake and release reactions have not been directly detected. Thus, their timing and the relevant intermediates have been suggested from indirect observations. The flash-induced absorbance changes reveal faster formation of an O intermediate with a higher  $Na^+$  concentration<sup>11,14-15</sup>. This acceleration suggests the  $Na^+$  uptake during the O formation. The subsequent intermediate (hereafter designated as NaR') has almost the same absorption spectrum as the dark state<sup>16</sup>, suggesting that  $Na^+$  is already absent in NaR', at least around the retinal. Thus,  $Na^+$  is supposed to be captured and released during the formation and decay of O. However, these assignments seem to be somewhat inconsistent with the behavior of O decay reported for an NaR from the eubacterium *Gillisia limnaea* (GLR)<sup>14</sup>: Similar to its formation, its O decay also becomes faster as the  $Na^+$  concentration increases. Concerning the  $Na^+$  uptake, a different timing was also suggested by the QM/MM study, which assigned it to the formation of earlier intermediates (K or L) but not to O formation<sup>17</sup>. On the other hand, the  $Na^+$  involvement at O has been supported by recent structural analyses, where  $Na^+$  was identified around the PSB in the structures assigned to O<sup>18-19</sup>. These structures are in clear contrast to those in the nonphotolyzed states, in which  $Na^+$  is not identified inside the protein<sup>12-13</sup>.

Here, we show direct detection of the  $Na^+$ -capture and release processes. By using a  $Na^+$ -selective membrane, we detected transient  $Na^+$  concentration changes associated with  $Na^+$  uptake and release reactions during a single transport cycle. These timings closely match the formation and decay of O, which was detected by the flash-induced absorbance changes.

## MATERIALS AND METHODS

**Sample preparation.** *Escherichia coli* strain DH5 $\alpha$  was used for DNA manipulation. Throughout this study, we used a NaR called GLR, which was mentioned above. The GLR gene (GenBank accession no. EHQ02967) with codons optimized for *E. coli* expression was chemically synthesized (Funakoshi, Tokyo, Japan) and inserted into the Nde I/Xho I site of the pET-21c vector (Merck). This plasmid results in GLR with additional amino acids in the C terminus (-LEHHHHHH). Using almost the same procedure, a proteorhodopsin (PR) gene was inserted into the pET plasmid. The PR gene sequence is identical to that in a plasmid reported previously<sup>20</sup>. The D116N mutation was introduced into GLR using the QuikChange site-directed mutagenesis kit (Stratagene, La Jolla, CA, USA). The DNA sequences were confirmed by a standard method using an automated DNA sequencer (Model 3100; Applied Biosystems, Foster City, CA, USA). The protein expression, purification, and the lipid reconstitution were performed as previously described<sup>21-23</sup>. Briefly, the proteins were expressed in the presence of 10  $\mu$ M all-*trans* retinal into the cell membranes of *E. coli* BL21(DE3) cells. After solubilization with the detergent n-dodecyl  $\beta$ -D-maltopyranoside (DDM), the solubilized proteins were purified by Ni-NTA chromatography in the presence of 0.05–0.1% DDM. The purified proteins were mixed with a suspension of phosphatidylcholine (PC) from egg yolk

(Avanti, Alabaster, AL, USA) at a protein: PC molar ratio of 1:30. After incubation for 1 h at room temperature, the detergent was removed by gentle stirring overnight (4  $^{\circ}$ C) in the presence of SM2 Adsorbent Bio-Beads (Bio-Rad, Hercules, CA, USA). The reconstituted proteins were separated from the Bio-Beads by filtration and then collected by centrifugation.

**Measurements with a  $Na^+$ -selective membrane.** A polyvinyl chloride (PVC)-based membrane was prepared using bis(12-crown-4) (Dojindo Lab, Kumamoto, Japan) and o-nitrophenyloctylether (NPOE) for the  $Na^+$  ionophore and the plasticizer, respectively. PVC (average polymerization degree, 1050) was purchased from Wako Chemicals (Osaka, Japan) and used without further purification. The PVC (80 mg), Bis(12-crown-4) (8 mg) and NPOE (160 mg) were dissolved in tetrahydrofuran (2.4 ml). The solution was poured into a Petri dish (5.9  $cm^2$  in area), and the solvent was evaporated at room temperature. The resulting membrane was transparent and approximately 0.1–0.2 mm thick.

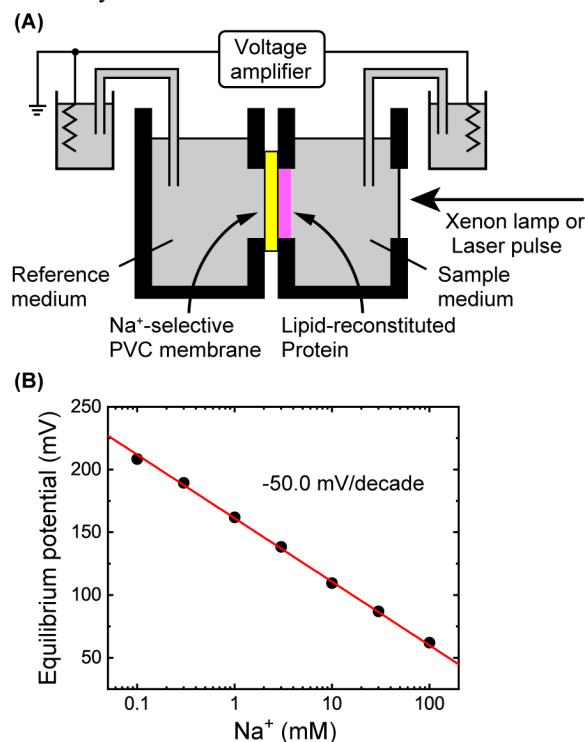


Figure 1. Schematic description of the photochemical cell used in this study (A) and the  $Na^+$ -concentration responses of the bare  $Na^+$ -selective membrane (B).

The schematic illustration of the electrochemical cell is shown in Fig. 1A. This cell consists of two Teflon chambers with holes (5 mm in diameter), which were the same as those described by Muneyuki et al.<sup>24</sup>. A disk 10 mm diameter was cut from the PVC membrane and inserted in the holes between the chambers. The "sample" chamber has another hole for the light-activation experiments. For the experiments using proteins, the assembled cell was first placed on its side so that the lipid-reconstituted proteins could be deposited horizontally onto the PVC membrane. For deposition, the reconstituted proteins were suspended in distilled water with a protein concentration of 10  $\mu$ M, where we assumed a molar extinction coefficient of 45,000  $M^{-1} cm^{-1}$  at the respective  $\lambda_{max}$ . The suspensions of 50  $\mu$ L were applied on the surface of the PVC membrane, followed by the

evaporation of water under reduced pressure to produce a dried film. This procedure was performed in duplicate. As a result, approximately 1.0 nmol of proteins were deposited on the PVC membrane. These proteins were tightly bound to the membrane, and their detachment was negligible during the following experiments.

The basal buffer solution for the membrane potential measurements was 50 mM Tris-HCl, pH 8.5. Before all measurements, both chambers were filled with a buffer containing 1 M NaCl and incubated for 1 h for the conditioning of the PVC membrane. Then, the buffer solution in the sample chamber was replaced with a buffer containing the appropriate concentration of NaCl, which was made by mixing the 100 mM NaCl and 100 mM KCl buffers so that the ionic strength was kept constant. After any replacements of the buffers, the samples were left for 5 min to equilibrate. All measurements were performed at room temperature (~25 °C).

For activation of the proteins, two light sources were used. The source for 1 sec illumination was a 150 W Xenon arc lamp in combination with three glass filters (IRA-25S, KL-53 and Y-46; Toshiba, Tokyo, Japan), which provided green light with a maximum intensity at approximately 530 nm. The light duration was controlled by a mechanical shutter. The source for a 5 nsec flash (532 nm, 1.2 mJ/pulse) was a second harmonic of a Q-switched Nd:YAG laser (Minilite I, Continuum, San Jose, CA, USA). In both cases, the light-induced potential changes were measured by using a homemade amplifier (response time ~ 9  $\mu$ sec), which was equipped with a 0.033 Hz low cut filter for the elimination of the baseline drift. For the calculations of the light-induced potential changes, the data before illumination were adopted as baselines. To improve the S/N ratio, the signals were averaged over 10 times for 1 sec illumination and 100 times for a 5 nsec flash, respectively.

**Measurements of flash-induced absorbance changes.** The suspensions of the reconstituted proteins were activated by a 7 nsec laser pulse (532 nm, 5 mJ), and the subsequent absorbance changes were recorded with a single wavelength kinetic system. The details of the apparatus are described elsewhere<sup>25</sup>. To improve the S/N ratio, 30 laser pulses were used at each measurement wavelength. The buffer solutions were the same as those for the membrane potential measurements. All data were obtained at 25 °C.

## RESULTS AND DISCUSSION

**Application of the Na<sup>+</sup>-selective membrane for the Na<sup>+</sup>-transfer reactions.** For H<sup>+</sup>-pump rhodopsins, the timing of H<sup>+</sup> release and uptake have been conventionally detected by a pH indicator dye pyranine<sup>26-28</sup>. During a single photocycle, the H<sup>+</sup> pump induces a H<sup>+</sup> concentration change due to the time difference between H<sup>+</sup> release at the EC side and the H<sup>+</sup> uptake at the CP side. This change in H<sup>+</sup> concentration is ordinarily 0.1–1  $\mu$ M, which is near to or larger than the dissociation constant of pyranine for H<sup>+</sup> (~0.05  $\mu$ M)<sup>29</sup>. Thus, pyranine causes a detectable absorbance change in response to the H<sup>+</sup> release and uptake reactions. For Na<sup>+</sup>, indicator dyes are also commercially available. However, their dissociation constants (4–200 mM) are significantly higher than that of pyranine<sup>29</sup>. Thus, the detection of the Na<sup>+</sup> concentration change is difficult unless we can concentrate NaR to an unusually high level and can photoactivate it with high efficiency. Instead of these indicator dyes, we herein employed the Na<sup>+</sup>-selective membrane, which is a PVC membrane involving the Na<sup>+</sup>

ionophore. When two solutions are separated with this membrane as shown in Fig. 1A, the partitioning of Na<sup>+</sup> occurs at two solution/membrane interfaces, which lead to the respective phase-boundary potentials. Within the membrane, the Na<sup>+</sup>-ionophore complex distributes equally, and so the potential difference does not exist. As a result, the membrane potential ( $\Psi$ ) is governed by the sum of two phase-boundary potentials and thus described by the Nernst equation<sup>30</sup>:

$$\Psi \text{ (mV)} = -59.2 \log \frac{[\text{Na}^+]}{[\text{Na}^+]_{\text{ref}}} \quad (\text{at } 25.0 \text{ }^\circ\text{C}) \quad (1)$$

where  $\Psi$  stands for the electric potential of the sample medium with respect to that of the reference medium, and  $[\text{Na}^+]$  and  $[\text{Na}^+]_{\text{ref}}$  represent the Na<sup>+</sup> concentrations in these mediums, respectively. For the detection of Na<sup>+</sup> transfer reactions, we deposited the lipid-reconstituted NaR on one side of the membrane so that the illumination induces a large change in Na<sup>+</sup> concentration near the PVC membrane. In response to the Na<sup>+</sup> concentration change, the phase-boundary potential also changes at this side, which in turn causes the change of membrane potential. The change of phase-boundary potential occurs very rapidly. Thus, the membrane potential can follow the light-induced change in the Na<sup>+</sup> concentration.

For the lipid reconstitution, we employed a high protein to lipid ratio (NaR: lipid = 1: 30). Thus, NaR was incorporated into the lipid membrane fragment, not into the spherical liposome. As a result, the light-induced change in Na<sup>+</sup> concentration should reflect the order of Na<sup>+</sup> uptake and release during the transport cycle. If the uptake occurs first followed by release, the Na<sup>+</sup> concentration should decrease under illumination. On the other hand, if the release occurs first followed by uptake, the Na<sup>+</sup> concentration should increase.

Many microbial rhodopsins are known to adopt oligomeric states in the cell membranes. Concerning the lipid-reconstituted NaR, the high-speed AFM imaging proved its pentameric state<sup>31</sup>, whose assembly was essentially the same with that observed in the crystal structure<sup>13</sup>. Thus, NaR used in this study probably takes pentameric state.

**Na<sup>+</sup>-concentration response of the bare Na<sup>+</sup>-selective membrane.** First, we tested the response of a bare Na<sup>+</sup>-selective membrane. In Fig. 1B, the membrane potential is plotted against the Na<sup>+</sup> concentrations in the sample medium while keeping the Na<sup>+</sup> concentration at 1 M for the reference medium. This figure shows a slope of -50.0 mV/decade, which is close to the ideal Nernstian slope of -59.2 mV/decade. The reason for the slight difference is not known. However, the slope is almost constant over a wide Na<sup>+</sup> concentration range, indicating that the PVC membrane actually senses the Na<sup>+</sup> concentration.

**Na<sup>+</sup>-concentration change due to the Na<sup>+</sup>-transfer reactions.** Next, we examined the effect of a continuous illumination on the membrane potential. For the bare membrane, no changes were observed (data not shown). However, as shown in Fig. 2A, a positive potential change was observed for the membrane covered with NaR. Here, the NaR was deposited on the membrane surface facing the sample medium, indicating that the photolyzed NaR induces a decrease in Na<sup>+</sup> concentration. Therefore, NaR surely captures Na<sup>+</sup> after photoactivation. The potential change has a shape weakly differentiated, reflecting a weak low cut filter (0.033 Hz) involved in the amplifier. This differentiated shape is close to the output when we input the square wave voltage into the amplifier (Fig. S1). Thus, the "true" change in Na<sup>+</sup> concentration should also be close to the square shape. The potential changes

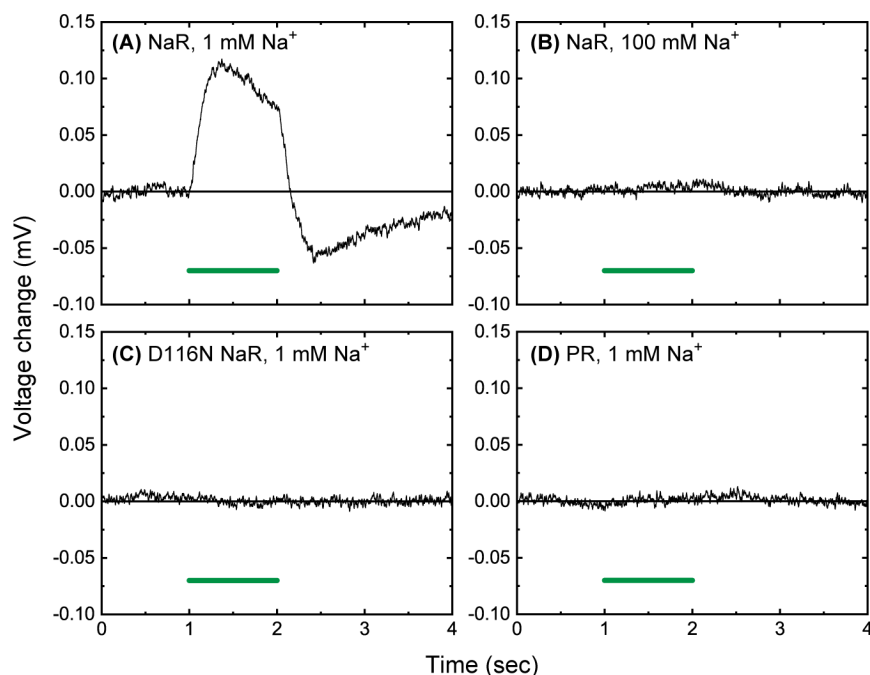


Figure 2. Potential change of Na<sup>+</sup>-selective membrane under continuous illumination. The membrane surfaces were covered with the lipid-reconstituted NaR (A and B), its D116N mutant (C), and PR (D), respectively. The green bar indicates the period of illumination and the Na<sup>+</sup> concentrations in the sample mediums are indicated in the panels.

at various Na<sup>+</sup> concentrations are shown in Fig. S2. With increasing Na<sup>+</sup> concentration, the potential change became larger, reflecting the increase of NaR molecules undergoing the Na<sup>+</sup>-pumping photocycle. However, the potential change began to decrease with further increases in Na<sup>+</sup> concentration and finally disappeared at 100 mM Na<sup>+</sup> (Fig. 2B and Fig. S2). This behavior reflects that the potential change ( $\Delta\psi$ ) depends on not only the light-induced change in Na<sup>+</sup> concentration ( $\Delta[\text{Na}^+]$ ) but also the Na<sup>+</sup> concentration in the bulk solution ( $[\text{Na}^+]$ ). This relationship is theoretically described by Eq. 2,

$$\Delta\psi \text{ (mV)} = -50.0 \log(1 + \Delta[\text{Na}^+]/[\text{Na}^+]) \quad (2)$$

where the coefficient of "-50.0" represents the slope in Fig. 1B. At a high Na<sup>+</sup> concentration ( $[\text{Na}^+]$ ), the value of  $\Delta[\text{Na}^+]/[\text{Na}^+]$  is almost zero, and thus the  $\Delta\psi$  becomes negligible ( $\Delta\psi = -50.0 \log(1) = 0$ ).

During the NaR deposition, NaR might orient in a specific direction. If this is the case, the electrogenicity might be induced under illumination and then might contribute to the potential change. However, this potential change should remain even at a high Na<sup>+</sup> concentration. Thus, a negligible potential change at a high Na<sup>+</sup> concentration (Fig. 2B) reflects that the PVC membrane senses only the change in Na<sup>+</sup> concentration. This consideration was further confirmed by using D116N NaR and the H<sup>+</sup> pump PR. As shown in Fig. 2C and D, no potential changes were observed in both cases. The D116 residue is located near PSB (Fig. S3A) and its replacement by Asn is known to remove the Na<sup>+</sup>-pump activity<sup>11</sup>. The data for PR (Fig. 2D) indicates no sensitivity of the PVC membrane against the local pH change. NaR is called a "hybrid pump", because NaR pumps H<sup>+</sup> if the medium contains neither Na<sup>+</sup> nor Li<sup>+</sup><sup>11</sup>. As shown in Fig. S4, this feature is also preserved in the GLR used in this study. Thus, at a lower Na<sup>+</sup> concentration, most GLR acts as a H<sup>+</sup> pump. Even in this condition, the membrane potential

reflects only the change in Na<sup>+</sup> concentration evoked by the GLR undergoing a Na<sup>+</sup>-pump cycle.

**Intermediates associated with the Na<sup>+</sup> uptake and release reactions.** For the identification of the intermediates, two kinds of data were obtained using nanosecond laser pulses: One is the flash-induced transient absorbance change, and the other is the flash-induced membrane potential change.

Figure 3A, B, and C show the flash-induced absorbance changes measured at typical three wavelengths. Here, eight traces with 0–30 mM Na<sup>+</sup> are plotted simultaneously. Due to the fast decay, the earliest intermediate K was not observed by our apparatus. Instead, the blueshifted intermediates, which were previously assigned to L and the subsequent M, were first observed at 410 nm (Fig. 3A). With concomitant decay of their equilibrium, the redshifted O appears at 590 nm (Fig. 3B). Another absorbance change at 510 nm reflects the depletion and recovery of the dark state through the last intermediate NaR' (Fig. 3C). This photocycle scheme is summarized in Fig. S3B. As described above, O has been considered to involve Na<sup>+</sup> inside the protein. By elevating the Na<sup>+</sup> concentration, the accumulation of O becomes prominent, and the peak position shifts to an earlier time (Fig. 3B). Thus, the next concern is whether the changes in membrane potential match with the accumulation of O at any Na<sup>+</sup> concentration in terms of both amplitude and timing.

As shown in Fig. 3B, even at 0 mM Na<sup>+</sup>, the O-like intermediate appears at 590 nm. This "pseudo" O is the intermediate appearing in the H<sup>+</sup> pumping cycle. As the Na<sup>+</sup> concentration increases, the contribution of another O, which appears in the Na<sup>+</sup>-pumping cycle, becomes dominant. For the comparison with the membrane potential signals, we removed the contributions of the "pseudo" O from the measured absorbance changes as described below. Compared to the

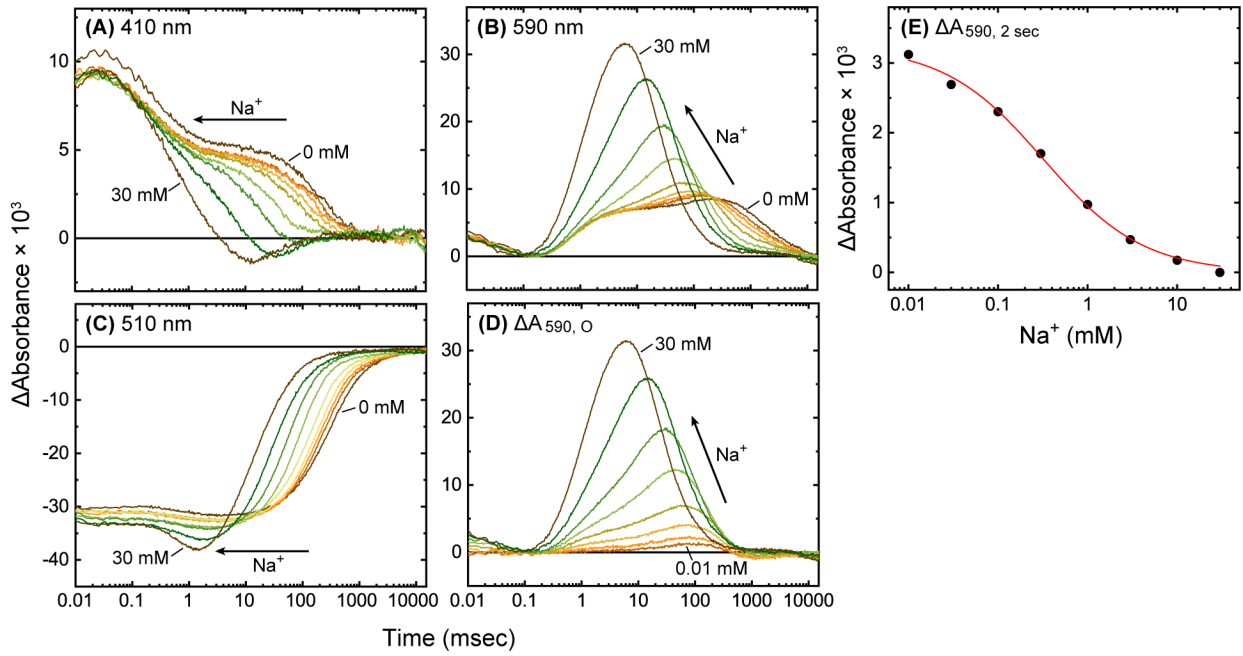


Figure 3. Flash-induced absorbance changes of NaR. In Panels A-C, the time-dependent changes at the typical three wavelengths are plotted. The  $\text{Na}^+$  concentrations are 0, 0.01, 0.03, 0.1, 0.3, 1, 3, 10, and 30 mM, respectively. Panel D shows the calculated absorbance changes reflecting only the accumulation of O in the  $\text{Na}^+$ -pumping cycle. These calculations used the fitting results in Panel E, where the absorbance changes at 2 sec in Panel B were plotted against  $\text{Na}^+$  concentration. The smooth line is the best fitted result with Eq. 3. For details, see the text.

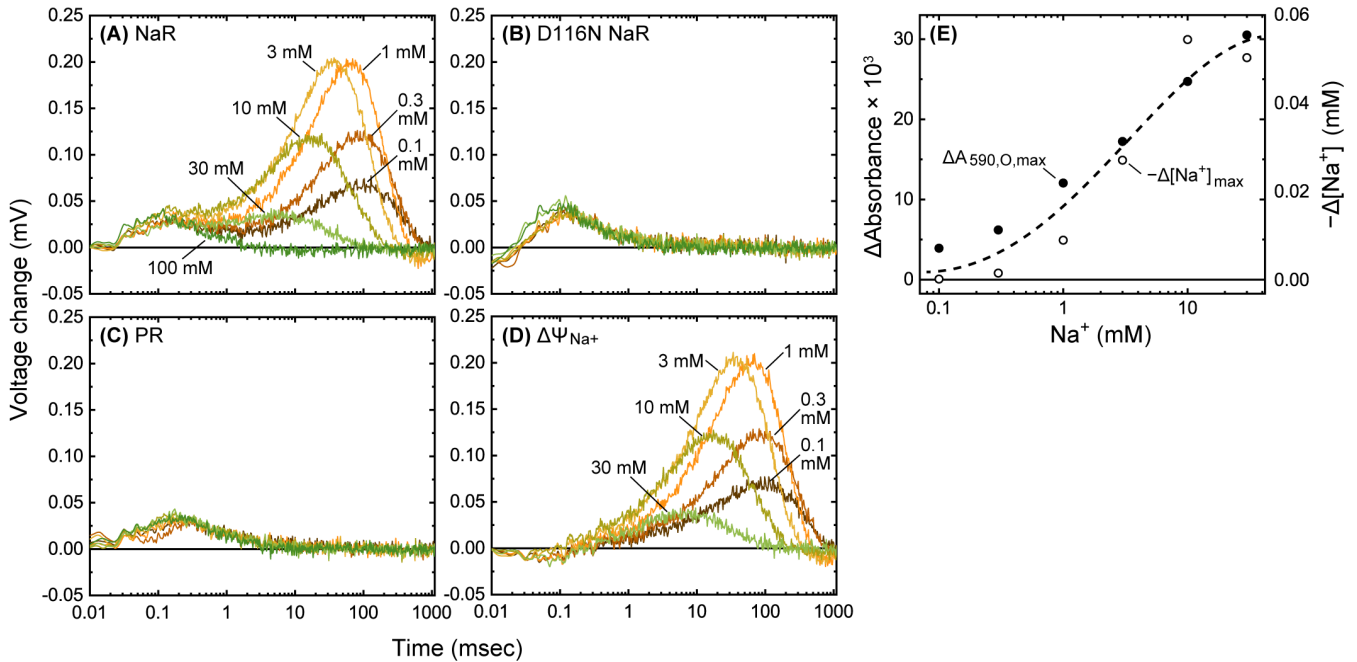


Figure 4. Flash-induced potential changes of the  $\text{Na}^+$ -selective membrane. The membrane surfaces were covered with the lipid-reconstituted NaR (A), its D116N mutant (B), and PR (C), respectively. Panel D shows the remaining potential changes for wild-type NaR after subtraction of trace at 100 mM  $\text{Na}^+$ . The peak values in this panel were picked up and then used for the calculations of the corresponding  $\text{Na}^+$ -concentration changes ( $\Delta[\text{Na}^+]_{\text{max}}$ ). The calculated values were plotted in Panel E (open circles) together with the peak values of the traces in Fig. 3D ( $\Delta A_{590, O, \text{max}}$ , filled circles). For details, see the text.

"pseudo" O, the other O has a faster decay rate. Thus, the positive absorbance changes in the late time region ( $> 1$  sec) reflect only the accumulations of the "pseudo" O. In Fig. 3E, the absorbance changes at 2 sec ( $\Delta A_{590, 2 \text{ sec}}$ ) are plotted against the  $\text{Na}^+$  concentration. Here, the smooth line is the best fitting result with the equation:

$$\Delta A_{590, 2 \text{ sec}} = \Delta A_0 \times f_{\text{O-like}} = \Delta A_0 / (1 + [\text{Na}^+]^n / K_{0.5}^n) \quad (3)$$

where  $\Delta A_0$  and  $n$  represent the  $\Delta A_{590, 2 \text{ sec}}$  at 0 mM  $\text{Na}^+$  and Hill coefficient, and  $K_{0.5}$  stands for the  $\text{Na}^+$  concentration at which the photocycle branching is at its midpoint, respectively. These determined values are  $\Delta A_0 = 3.24$  mABS,  $n = 0.78$  and  $K_{0.5} = 0.32$  mM. In Eq. 3,  $f_{\text{O-like}}$  represents the mole fraction of "pseudo" O. By using the  $f_{\text{O-like}}$  values, the absorbance changes reflecting only O ( $\Delta A_{590, \text{O}}(t)$ ) were estimated by:

$$\Delta A_{590, \text{O}}(t) = \Delta A_{590}(t) - f_{\text{O-like}} \times \Delta A_{590, 0 \text{ mM}}(t) \quad (4)$$

where  $\Delta A_{590}(t)$  and  $\Delta A_{590, 0 \text{ mM}}(t)$  represent the raw data at 590 nm measured at the corresponding  $\text{Na}^+$  concentration and at 0 mM  $\text{Na}^+$ , respectively. The calculated  $\Delta A_{590, \text{O}}(t)$  are plotted in Fig. 3D.

Previously, Balashov *et al.* also determined the  $K_{0.5}$  value for GLR with similar procedure<sup>14</sup>. Their determined value is 60  $\mu\text{M}$  and thus significantly lower than our value (0.32 mM). This difference might originate from the different buffer conditions. They varied  $\text{Na}^+$  concentration without the ionic strength adjustment. On the other hand, we kept the ionic strength at the constant value equivalent to 100 mM NaCl by adding the KCl salt. Indeed, when we did not add KCl salt, the  $K_{0.5}$  value became very small  $\sim 90$   $\mu\text{M}$  (data not shown). Thus, the ionic strength and/or  $\text{K}^+$  ion might affect the  $\text{Na}^+$  concentration for the photocycle branching.

Figure 4A shows the flash-induced potential changes in the  $\text{Na}^+$ -selective membrane covered by wild-type NaR. At approximately 10–100 msec, relatively large peaks appeared. As shown in Fig. 3D, O accumulation also reaches its maximum in the same time region. Thus,  $\text{Na}^+$  is probably involved at O. As the  $\text{Na}^+$  concentration increases, the peak magnitude first increased and then decreased. Finally, the peak disappeared at 100 mM  $\text{Na}^+$ , indicating that this potential change surely originates from the  $\text{Na}^+$  concentration change. In Fig. 4A, another small peak also appeared at approximately 0.1 msec. At any  $\text{Na}^+$  concentration, this peak appeared with the same shape and the same amplitude. Similar peaks were also observed for D116N NaR and PR (Fig. 4B and C). Thus, these peaks are not associated with the  $\text{Na}^+$ -pumping reaction. Microbial rhodopsins and visual rhodopsin are known to show light-induced charge displacements by only their conformational changes, even though these conformational changes do not involve ion transfer reactions<sup>32</sup>. These simple charge displacements might induce potential changes of the PVC membrane, if the proteins are oriented in a specific direction. This type of potential change should remain even at high  $\text{Na}^+$  concentration as similar to the peaks at approximately 0.1 msec. However, if the NaR is indeed oriented, the latter peak at 10–100 msec should also remain due to its electrogenicity, because the latter peak surely originates from the  $\text{Na}^+$ -transfer reactions. Thus, at present, the origin of the first peak is not known. Although this uncertainty, the first peak does not relate with the  $\text{Na}^+$  uptake and release reactions. Thus, we subtracted the first peak from the potential change for the comparison with the flash-induced absorbance change. The calculated potential changes (designated as  $\Delta \Psi_{\text{Na}^+}$ ) are shown in Fig. 4D, where the

potential change at 100 mM  $\text{Na}^+$  was subtracted from the potential changes at other  $\text{Na}^+$  concentrations.

If O is the intermediate involving  $\text{Na}^+$  inside the protein, its amount of accumulation should be proportional to the decreased  $\text{Na}^+$  concentration ( $\Delta[\text{Na}^+]$ ). Thus, we compared these values in Fig. 4E. The filled circles represent the maximum absorbance changes in Fig. 3D ( $\Delta A_{590, \text{O, max}}$ ), which indicate the maximum accumulations of O at respective  $\text{Na}^+$  concentrations. The open circles represent the magnitude of the maximum decreases of  $\text{Na}^+$  concentration ( $-\Delta[\text{Na}^+]_{\text{max}}$ ), which was calculated by the following equation:

$$\Delta[\text{Na}^+]_{\text{max}} = [\text{Na}^+] \cdot (10^{-\Delta \Psi_{\text{max}}/50.0} - 1) \quad (5)$$

This equation was derived from Eq. 2 and the  $\Delta \Psi_{\text{max}}$  represents the maximum potential changes of  $\Delta \Psi_{\text{Na}^+}$  (Fig. 4D) at respective  $\text{Na}^+$  concentration. As shown in Fig. 4E, these two values show almost the same  $\text{Na}^+$  dependency, indicating that O surely contains  $\text{Na}^+$  inside the protein.

Next, we compared the time courses of O accumulation and the  $\text{Na}^+$  concentration change. Each panel in Fig. 5 contains two time traces: They are the absorption changes in Fig. 3D ( $\Delta A_{590, \text{O}}$ ) and the membrane potential changes in Fig. 4D ( $\Delta \Psi_{\text{Na}^+}$ ), respectively. As shown here, two traces overlapped well in all panels, even though the peak positions gradually shifted depending on the  $\text{Na}^+$  concentration. These results also emphasized that  $\text{Na}^+$  is captured and released during the formation and decay of the O intermediate.

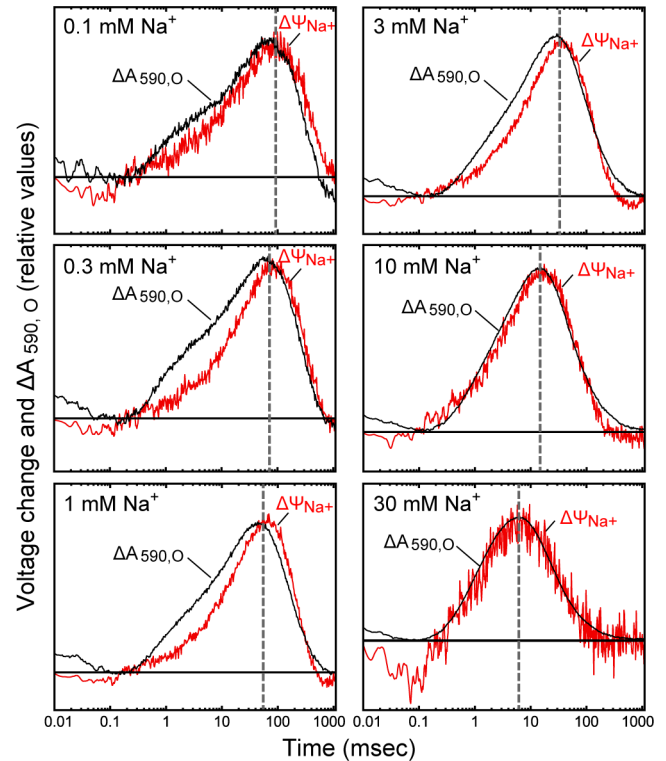


Figure 5. Comparisons of time courses of O accumulations and  $\text{Na}^+$  concentration changes. The traces in Fig. 3D and Fig. 4D were plotted together with the adjusted y-axis. The two traces show almost the same time course at all  $\text{Na}^+$  concentrations. The vertical broken lines indicate the peak positions for the clarity of their time shifts depending on the  $\text{Na}^+$  concentration.

At low Na<sup>+</sup> concentrations (0.1 – 1 mM), two traces in Fig. 5 do not perfectly match, where the Na<sup>+</sup> uptakes (red traces) are slower than the formations of O (black traces). These differences might be caused by the contaminations of "pseudo" O in the black traces. As shown in Fig. 3B, the raw data of  $\Delta A_{590}(t)$  at 0 mM, which involves only the "pseudo" O, has two peaks around 1-10 msec and 10-100 msec, respectively. On the other hand, at lower Na<sup>+</sup> concentrations, the black traces in Fig. 5 have shoulders around 1-10 msec, which is similar to the first peak of "pseudo" O. For the calculations of the black traces, we assumed that the time course of "pseudo" O does not change even varying the concentrations of Na<sup>+</sup> and/or K<sup>+</sup>. This assumption might not be correct. If the magnitude of the first peak is altered, this peak is not completely removed by the subtraction. The remaining peaks might form the shoulders at lower Na<sup>+</sup> concentrations and then apparently enlarge the differences from the red traces.

**Na<sup>+</sup> uptake reactions.** As mentioned above, D116N NaR completely loses its Na<sup>+</sup>-pumping activity<sup>11</sup>. This Asp residue is a counter ion of the PSB (Fig. S3A) and acts as a H<sup>+</sup> acceptor from the PSB. The resultant loss of the positive charge is considered to be essential for Na<sup>+</sup> passage over the Schiff base region and to allow the arrival of Na<sup>+</sup> at the putative binding site between N112 and D251 (Fig. S3A)<sup>4, 19, 33</sup>. In addition to this gating role, the D116 residue is also considered to directly interact with Na<sup>+</sup> before the movement over the Schiff base region<sup>17-18</sup>. Thus, this residue seems to be crucial for Na<sup>+</sup> binding inside the protein. Our observation in Fig. 2C and 4B proved this hypothesis. As shown here, no potential change was observed for D116N NaR, indicating that this mutant even lacks the Na<sup>+</sup> uptake ability. The D116 residue is located deep inside the protein and is approximately 18 Å away from the protein surface (Fig. S3A). Despite this long distance, the Na<sup>+</sup> seems to come around D116 by a single step movement during the O formation. The pathway in the CP channel should be narrow and highly hydrophobic<sup>12-13</sup>. Thus, NaR seems to have a mechanism to facilitate the Na<sup>+</sup> movement. One possibility is a transient hydration of the CP channel. Significant hydrations were indeed reported for other ion pump rhodopsins<sup>34-36</sup>.

## CONCLUSION

In this study, we detected small Na<sup>+</sup> concentration changes associated with the uptake and release reactions of NaR during its single transport cycle. The detected changes in Na<sup>+</sup> concentration closely matched with the O intermediate accumulations in terms of both amplitude and timing. Thus, we proved that Na<sup>+</sup> is captured and released during the formation and decay of O. As mentioned above, the transporters should assume different conformations for substrate uptake and the release. Thus, there seems to exist at least two O intermediates. We previously reported that the Na<sup>+</sup>-pumping cycle contains two subsequent redshifted intermediates and named them O1 and O2, respectively<sup>16</sup>. Thus, detailed characterizations of these intermediates should be performed in future investigation. Here, we employed an ion-selective membrane for the identification of the intermediate associated with the ion uptake and release reactions. This membrane is also a powerful tool for further analyses of ion transporters because we can probe the roles of individual amino acids in more detail. For example, if we find a mutant preserving the ion uptake ability but lacking the ion transport activity, the mutated residue clearly plays an essential

role in a process after the ion uptake. For NaR, analyses using various mutants are currently underway in our laboratory.

## ASSOCIATED CONTENT

### Supporting Information

The Supporting Information is available free of charge on the ACS Publications website.

The response of the voltage amplifier for the input of square wave voltage (Fig. S1), Light-induced potential changes of the Na<sup>+</sup>-selective membrane at various Na<sup>+</sup> concentrations (Fig. S2), Positions of key residues for putative Na<sup>+</sup> binding sites and the photocycle scheme of NaR (Fig. S3), Light-induced pH changes of suspensions of *E. coli* cells expressing GLR (Fig. S4) (PDF)

## AUTHOR INFORMATION

### Corresponding Author

\*Takashi Kikukawa

E-mail: kikukawa@sci.hokudai.ac.jp

### Notes

The authors declare no competing financial interest.

## ACKNOWLEDGMENTS

We thank Dr. Naoki Kamo for helpful discussion. This work was supported by JSPS KAKENHI granted to T.K. (17K07326) and by the Global Station for Soft Matter, a project of the Global Institution for Collaborative Research and Education at Hokkaido University.

## REFERENCES

- (1) Jardetzky, O., Simple allosteric model for membrane pumps. *Nature* **1966**, *211* (5052), 969-970.
- (2) Ernst, O. P.; Lodowski, D. T.; Elstner, M.; Hegemann, P.; Brown, L. S.; Kandori, H., Microbial and animal rhodopsins: structures, functions, and molecular mechanisms. *Chem. Rev.* **2014**, *114* (1), 126-163.
- (3) Spudich, J. L.; Sineshchekov, O. A.; Govorunova, E. G., Mechanism divergence in microbial rhodopsins. *Biochim. Biophys. Acta Bioenerg.* **2014**, *1837* (5), 546-552.
- (4) Kandori, H.; Inoue, K.; Tsunoda, S. P., Light-Driven Sodium-Pumping Rhodopsin: A New Concept of Active Transport. *Chem. Rev.* **2018**, *118* (21), 10646-10658.
- (5) Balashov, S. P., Protonation reactions and their coupling in bacteriorhodopsin. *Biochim. Biophys. Acta* **2000**, *1460* (1), 75-94.
- (6) Lanyi, J. K., Bacteriorhodopsin. *Annu. Rev. Physiol.* **2004**, *66*, 665-688.
- (7) Kolbe, M.; Besir, H.; Essen, L. O.; Oesterhelt, D., Structure of the light-driven chloride pump halorhodopsin at 1.8 Å resolution. *Science* **2000**, *288* (5470), 1390-1396.
- (8) Kouyama, T.; Kanada, S.; Takeguchi, Y.; Narusawa, A.; Murakami, M.; Ihara, K., Crystal structure of the light-driven chloride pump halorhodopsin from *Natronomonas pharaonis*. *J. Mol. Biol.* **2010**, *396* (3), 564-579.
- (9) Hayashi, S.; Tamogami, J.; Kikukawa, T.; Okamoto, H.; Shimono, K.; Miyauchi, S.; Demura, M.; Nara, T.; Kamo, N., Thermodynamic parameters of anion binding to halorhodopsin from *Natronomonas pharaonis* by isothermal titration calorimetry. *Biophys. Chem.* **2013**, *172*, 61-67.
- (10) Jung, K. H. In *New type of cation pumping microbial rhodopsins in marine bacteria*, 244th ACS National Meeting & Exposition, Philadelphia, PA, August 19-23, 2012, Abstract 271.
- (11) Inoue, K.; Ono, H.; Abe-Yoshizumi, R.; Yoshizawa, S.; Ito, H.; Kogure, K.; Kandori, H., A light-driven sodium ion pump in marine bacteria. *Nat. Commun.* **2013**, *4*, 1678.

- (12) Kato, H. E.; Inoue, K.; Abe-Yoshizumi, R.; Kato, Y.; Ono, H.; Konno, M.; Hososhima, S.; Ishizuka, T.; Hoque, M. R.; Kunitomo, H.; Ito, J.; Yoshizawa, S.; Yamashita, K.; Takemoto, M.; Nishizawa, T.; Taniguchi, R.; Kogure, K.; Maturana, A. D.; Iino, Y.; Yawo, H.; Ishitani, R.; Kandori, H.; Nureki, O., Structural basis for Na<sup>+</sup> transport mechanism by a light-driven Na<sup>+</sup> pump. *Nature* **2015**, *521* (7550), 48-53.
- (13) Gushchin, I.; Shevchenko, V.; Polovinkin, V.; Kovalev, K.; Alekseev, A.; Round, E.; Borsheveskiy, V.; Balandin, T., Crystal structure of a light-driven sodium pump. *Nat. Struct. Mol. Biol.* **2015**, *22*, 390-395.
- (14) Balashov, S. P.; Imasheva, E. S.; Dioumaev, A. K.; Wang, J. M.; Jung, K. H.; Lanyi, J. K., Light-Driven Na<sup>+</sup> Pump from *Gillisia limnaea*: A High-Affinity Na<sup>+</sup> Binding Site Is Formed Transiently in the Photocycle. *Biochemistry* **2014**, *53*, 7549-7561.
- (15) Kato, Y.; Inoue, K.; Kandori, H., Kinetic Analysis of H<sup>+</sup>-Na<sup>+</sup> Selectivity in a Light-Driven Na<sup>+</sup>-Pumping Rhodopsin. *J. Phys. Chem. Lett.* **2015**, *6* (24), 5111-5115.
- (16) Kajimoto, K.; Kikukawa, T.; Nakashima, H.; Yamaryo, H.; Saito, Y.; Fujisawa, T.; Demura, M.; Unno, M., Transient Resonance Raman Spectroscopy of a Light-Driven Sodium-Ion-Pump Rhodopsin from *Indibacter alkaliphilus*. *J. Phys. Chem. B* **2017**, *121* (17), 4431-4437.
- (17) Suomivuori, C. M.; Gamiz-Hernandez, A. P.; Sundholm, D.; Kaila, V. R. I., Energetics and dynamics of a light-driven sodium-pumping rhodopsin. *Proc. Natl. Acad. Sci. U. S. A.* **2017**, *114* (27), 7043-7048.
- (18) Kovalev, K.; Astashkin, R.; Gushchin, I.; Orekhov, P.; Volkov, D.; Zinovev, E.; Marin, E.; Rulev, M.; Alekseev, A.; Royant, A.; Carpentier, P.; Vaganova, S.; Zabelskii, D.; Baeken, C.; Sergeev, I.; Balandin, T.; Bourenkov, G.; Carpena, X.; Boer, R.; Maliar, N.; Borsheveskiy, V.; Büldt, G.; Bamberg, E.; Gordel'iy, V., Molecular mechanism of light-driven sodium pumping. *Nat. Commun.* **2020**, *11* (1), 2137.
- (19) Skopintsev, P.; Ehrenberg, D.; Weinert, T.; James, D.; Kar, R. K.; Johnson, P. J. M.; Ozerov, D.; Furrer, A.; Martiel, I.; Dworkowski, F.; Nass, K.; Knopp, G.; Cirelli, C.; Arrell, C.; Gashi, D.; Mous, S.; Wranik, M.; Gruhl, T.; Kekilli, D.; Brünle, S.; Deupi, X.; Schertler, G. F. X.; Benoit, R. M.; Panneels, V.; Nogly, P.; Schapiro, I.; Milne, C.; Heberle, J.; Standfuss, J., Femtosecond-to-millisecond structural changes in a light-driven sodium pump. *Nature* **2020**, *583* (7815), 314-318.
- (20) Tamogami, J.; Kikukawa, T.; Miyauchi, S.; Muneyuki, E.; Kamo, N., A tin oxide transparent electrode provides the means for rapid time-resolved pH measurements: application to photoinduced proton transfer of bacteriorhodopsin and proteorhodopsin. *Photochem. Photobiol.* **2009**, *85* (2), 578-589.
- (21) Hasemi, T.; Kikukawa, T.; Kamo, N.; Demura, M., Characterization of a Cyanobacterial Chloride-pumping Rhodopsin and Its Conversion into a Proton Pump. *J. Biol. Chem.* **2016**, *291* (1), 355-362.
- (22) Nakamura, S.; Kikukawa, T.; Tamogami, J.; Kamiya, M.; Aizawa, T.; Hahn, M. W.; Ihara, K.; Kamo, N.; Demura, M., Photochemical characterization of actinorhodopsin and its functional existence in the natural host. *Biochim. Biophys. Acta Bioenerg.* **2016**, *1857* (12), 1900-1908.
- (23) Hasemi, T.; Kikukawa, T.; Watanabe, Y.; Aizawa, T.; Miyauchi, S.; Kamo, N.; Demura, M., Photochemical study of a cyanobacterial chloride-ion pumping rhodopsin. *Biochim. Biophys. Acta Bioenerg.* **2019**, *1860* (2), 136-146.
- (24) Muneyuki, E.; Okuno, D.; Yoshida, M.; Ikai, A.; Arakawa, H., A new system for the measurement of electrogenicity produced by ion pumps using a thin polymer film: examination of wild type bacteriorhodopsin and the D96N mutant over a wide pH range. *FEBS Lett.* **1998**, *427* (1), 109-114.
- (25) Kikukawa, T.; Kusakabe, C.; Kokubo, A.; Tsukamoto, T.; Kamiya, M.; Aizawa, T.; Ihara, K.; Kamo, N.; Demura, M., Probing the Cl<sup>-</sup>-pumping photocycle of *pharaonis* halorhodopsin: Examinations with bacterioruberin, an intrinsic dye, and membrane potential-induced modulation of the photocycle. *Biochim. Biophys. Acta Bioenerg.* **2015**, *1847* (8), 748-758.
- (26) Heberle, J., Proton transfer reactions across bacteriorhodopsin and along the membrane. *Biochim. Biophys. Acta* **2000**, *1458* (1), 135-147.
- (27) Kikukawa, T.; Shimono, K.; Tamogami, J.; Miyauchi, S.; Kim, S. Y.; Kimura-Someya, T.; Shirouzu, M.; Jung, K. H.; Yokoyama, S.; Kamo, N., Photochemistry of *Acetabularia* rhodopsin II from a marine plant, *Acetabularia acetabulum*. *Biochemistry* **2011**, *50* (41), 8888-8898.
- (28) Iizuka, A.; Kajimoto, K.; Fujisawa, T.; Tsukamoto, T.; Aizawa, T.; Kamo, N.; Jung, K. H.; Unno, M.; Demura, M.; Kikukawa, T., Functional importance of the oligomer formation of the cyanobacterial H<sup>+</sup> pump *Gloeobacter* rhodopsin. *Sci. Rep.* **2019**, *9* (1), 10711.
- (29) Haugland, R. P., *The molecular probes handbook: A guide to fluorescent probes and labeling technologies*. 11th ed.; Life Technologies Corp.: Carlsbad, CA: 2010.
- (30) Bakker, E.; Bühlmann, P.; Pretsch, E., The phase-boundary potential model. *Talanta* **2004**, *63* (1), 3-20.
- (31) Shibata, M.; Inoue, K.; Ikeda, K.; Konno, M.; Singh, M.; Kataoka, C.; Abe-Yoshizumi, R.; Kandori, H.; Uchihashi, T., Oligomeric states of microbial rhodopsins determined by high-speed atomic force microscopy and circular dichroic spectroscopy. *Sci. Rep.* **2018**, *8* (1), 8262.
- (32) Skulachev, V., A single turnover study of photoelectric current-generating proteins. In *Method. Enzymol.*, Elsevier: 1982; Vol. 88, pp 35-45.
- (33) Inoue, K.; Konno, M.; Abe-Yoshizumi, R.; Kandori, H., The Role of the NDQ Motif in Sodium-Pumping Rhodopsins. *Angew. Chem., Int. Ed.* **2015**, *54* (39), 11536-11539.
- (34) Váró, G.; Lanyi, J. K., Effects of hydrostatic pressure on the kinetics reveal a volume increase during the bacteriorhodopsin photocycle. *Biochemistry* **1995**, *34* (38), 12161-12169.
- (35) Kikukawa, T.; Saha, C. K.; Balashov, S. P.; Imasheva, E. S.; Zaslavsky, D.; Gennis, R. B.; Abe, T.; Kamo, N., The lifetimes of *pharaonis phoborhodopsin* signaling states depend on the rates of proton transfers - Effects of hydrostatic pressure and stopped flow experiments. *Photochem. Photobiol.* **2008**, *84* (4), 880-888.
- (36) Shibusaki, K.; Shigemura, H.; Kikukawa, T.; Kamiya, M.; Aizawa, T.; Kawano, K.; Kamo, N.; Demura, M., Role of Thr218 in the light-driven anion pump halorhodopsin from *Natronomonas pharaonis*. *Biochemistry* **2013**, *52* (51), 9257-9268.

